ELSEVIER

Journal of Nuclear Materials 266–269 (1999) 1015–1019

journal of nuclear materials

B2-EIRENE code modelling of an island divertor

G. Herre, P. Grigull *, R. Schneider

Max-Planck-Institut für Plasmaphysik, EURATOM Association, Boltzmannstrasse 2, D-85748, Garching, Germany

Abstract

The multifluid plasma scrape-off layer transport code B2 coupled to the EIRENE Monte Carlo neutral gas transport code was applied to a prototypical island divertor configuration in W7-AS. The approach predicts the accessibility of stable, layer-like energy detachment within a relatively broad density range. The island geometry with typically small field line pitch has the beneficial effects of efficient shielding of the main plasma against neutrals, and of strong momentum losses from the power carrying layer due to momentum radial transport. The latter reduces the peak power load and eases detachment. The power exhaust properties and the onset of detachment can be positively affected by the choice of the field line pitch which can be varied in W7-AS by superimposed control fields.

Keywords: Stellarator; Island divertor; B2/EIRENE

1. Introduction

In the context of the development and near future operation of large stellarators (e.g. LHD and W7-X), the search for adequate power and particle exhaust scenarios comparable to those in tokamak divertors has become mandatory. A favoured option generally compatible with stellarator-specific confinement concepts is the island divertor which utilizes macroscopic magnetic islands at the plasma boundary in combination with adequately arranged targets and baffles for plasma exhaust. The islands can be produced by intrinsic (e.g. W7-AS, W7-X) or relatively small additional perturbation fields. Nevertheless, the suitability of this concept has not yet been proven. The relevant database is scarce and stems exclusively from few pre-investigations in CHS (local island divertor, LID)[1] and W7-AS (island configuration with inboard limiters) [2,3]. The present analysis applies the two-dimensional (2D) B2 (Braams) edge plasma transport code [4] linked with the EIRENE neutral transport code [5,6] to a specific W7-AS island divertor configuration but allows, nevertheless, to exemplarily assess crucial elements of the concept. The study is part of an ongoing island divertor programme which comprises, besides this 'proof of principle', the further development of a more adequate three-dimensional (3D) (Monte Carlo) edge transport code [3,7,8], the installation and study of a modular island divertor in W7-AS [3], and future investigations of an island divertor with flexible configuration in the W7-X device [9]. The paper continues previous studies [10] mainly by extending the parameter range to values relevant for detachment regimes. It addresses the questions whether in particular the extremely small field line pitch inside the islands and the neutral mean free path relative to the islands radial width allow to establish stable detachment at all in this approach, and to what degree island-specific (2D) effects affect the scenarios. The aim is to give a status report.

The following chapter briefly describes the W7-AS magnetic field configuration and grids used for numerical computation; free parameters and boundary conditions are specified in Section 3. In Section 4, the results are presented and discussed. Section 5 gives a summary of the results and draws conclusions.

2. Magnetic field configuration and numerical grids

The W7-AS configuration (major radius $R = 2$ m, minor radius $a = 0.18$ m, five magnetic field periods,

* Corresponding author. E-mail: grigull@ipp-garching.mpg.de

0022-3115/99/$ – see front matter
PII: S0022-3115(98)00557-1

$B \leqslant 2.5$ T, rotational transform $\iota = 0.3$–0.7, low magnetic shear) is, at $\iota = n/m > 0.4$, bounded by a chain of macroscopic magnetic islands of the symmetry $5/m$. The radial position, size and internal rotational transform ι_i of the islands can be controlled by the externally adjustable edge rotational transform ι_a, a superimposed vertical field and/or, in the near future divertor phase, by additional control fields which may also compensate finite-β effects. The planned island divertor is designed for configurations with $\iota_a \approx 5/9$ providing both, sufficient main plasma cross section and relatively large island dimensions (Fig. 1). For these reasons, this type was also chosen for the present analysis. In this case, the island cross sections shown in Fig. 1 belong to a unique island which closes after nine toroidal revolutions.

As stellarators like W7-AS are strongly non-axisymmetric, the application of the 2D B2 fluid approach requires helical averaging of the 3D edge structure. For that purpose the B2 geometric coefficients were derived from a 3D grid (with closest approximation to orthogonality) by helically averaging distances and integrating up areas and volumes. Periodical boundary conditions at the connection to poloidally neighboured islands and intercell connections along the symmetry line outside the o-point (corresponding to line JK in Fig. 2) were treated by three topological cuts in the B2 grid. The EIRENE grid (Fig. 2) was generated by geometrically averaging the island structure along the helical coordinate. Computations were performed in the standard way: B2 results mapped onto the EIRENE grid provided the EIRENE input; the resulting neutral distribution mapped onto the B2 grid provided the next iteration B2 source terms etc.

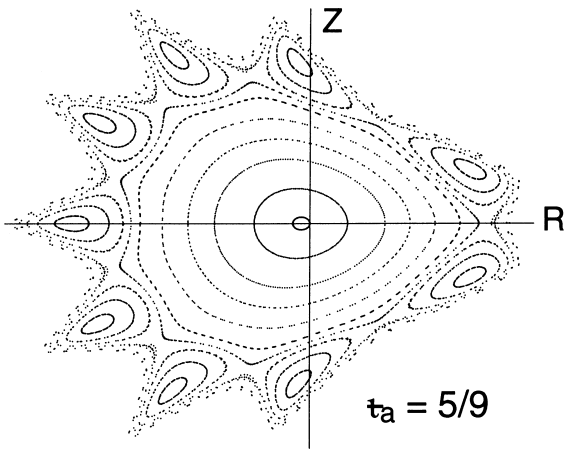

Fig. 1. Triangular cross section of the W7-AS magnetic field configuration with $n/m = 5/9$ boundary islands used for the B2-EIRENE code simulations. The cross sections change from triangular over elliptic to triangular with fivefold periodicity.

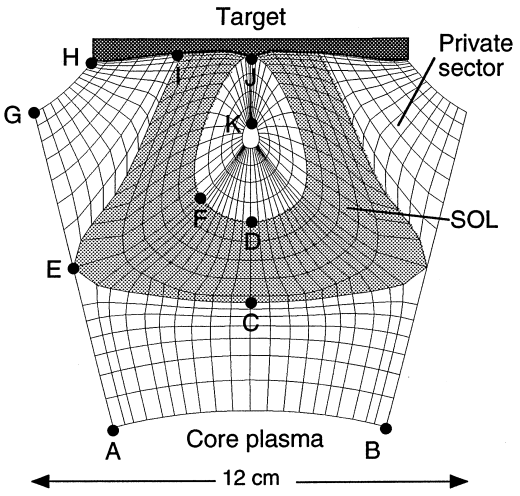

Fig. 2. Section of the EIRENE code numerical grid with points for text explanation. The grid is adapted to the helically averaged island structure.

3. Free parameters and boundary conditions

The B2 fluid approach solves the continuity, momentum and energy equations (details can be seen from Ref. [4]). Parallel transport is described by Navier–Stokes type equations; for the radial transport a diffusive Ansatz is made. Particle radial diffusion coefficients were chosen according to the empirical W7-AS scaling $D_\perp = 2P_S^{0.85}n_{es}^{-1.1}$ (with P_S being the net power crossing the separatrix in MW and n_{es} the upstream separatrix density in 10^{19} m^{-3}) up to $n_{es} = 3 \times 10^{19}$ m^{-3} [11]; above this density, $D_\perp$ was set to constant. Pinch velocities were assumed to be zero. The value of the electron anomalous heat diffusivity $\chi_{e\perp}$ was taken as three times $D_\perp$; the coefficient of anomalous cross field viscosity was set to $\eta_\perp = m_i n_e D_\perp$. At the inner grid boundary (line AB in Fig. 2), the total power outflux from the core P_c and the deuterium density were prescribed. Sheath boundary conditions [12] were used at the target plates. At the outside boundary of the private flux region (line GH), radial decay lengths (2 cm for densities and 3 cm for temperatures) have been fixed. Deuterium recycling coefficients were assumed to be $R = 1$ at the targets and $R = 0.98$ at the walls.

In order to elucidate effects of the island geometry under less complex conditions, the upstream separatrix density n_{es} was scanned first for pure deuterium plasmas at varied field line pitch at the edge and relatively low power, $P_c = 220$ kW. The pitch variation approximately covers the experimentally accessible range in W7-AS and includes the standard pitch distribution (without additional correction fields, denoted as 'medium pitch' in the following) and pitch values increased by a factor of four ('high pitch') or decreased by a factor of two ('low

pitch'). At the standard distribution, the pitch poloidally averaged along the grid cells just inside the island separatrix (see Fig. 2) is $\sin\theta = 0.002$; the corresponding field line connection length from the upstream stagnation point to the target is $L_c = 98$ m. The effect of impurity radiation is then shown at medium pitch by an n_{es} scan at $P_c = 600$ kW with self-consistent treatment of carbon as edge dominating, intrinsic impurity considering physical (TRIM code data [13]) and chemical sputtering from the carbon targets. The chemical sputtering efficiency was assumed to be 2% of the incoming particle flux.

4. Results and discussion

Pure deuterium plasmas. Fig. 3 plots divertor plasma parameters versus the upstream separatrix density n_{es}. At medium field line pitch (solid lines), the course of the downstream parameters T_{ed}^{max} (maximum electron temperature), n_{ed}^{max} (maximum electron density) and Γ_{pt} (particle flux onto target) indicate the transition from a linear regime to divertor high recycling at $n_{es} \approx 10^{19}$ m^{-3} and the onset of slight (energy) detachment at $n_{es} \approx 2.5 \times 10^{19}$. Above $n_{es} = 2 \times 10^{20}$ m^{-3}, volume recombination becomes strongly effective leading to complete detachment and unstationarity. The stable detachment scenarios show saturating n_{ed} and Γ_{pt} values, a divertor leakage for neutrals of about 1%, increasing divertor radiated power fractions f_r^{div} (Fig. 3(c)) and significant net momentum losses indicated by respective loss factors F_m (Fig. 3(d), for definitions see below). With increasing upstream density, the ionization front is found to quickly move away from the target towards the x-points as it is more or less typical also for tokamak divertor geometries. As Fig. 4 shows, the island geometry with small field line pitch and the two 'divertor tails' at close proximity (partially overlapping) involves, however, some characteristic features. Due to the specific 2D patterns in particular of energy and momentum flow, the downstream power carrying layer nearly homogeneously spreads over the scrape-off layer (SOL) between the two strike points as it is indicated by the parallel power flux $q_{\|d}$ profiles in Fig. 4(b) (peaking of the target thermal load q_t in the private sector (PS) is caused by increasing field line inclination in this range). The n_{ed} and in particular T_{ed} radial profiles are relatively flat over the whole n_{es} range (Fig. 4(a)) thus leading to a 'layer' type detachment without strong profile changes.

This behaviour shall be illustrated by some details of the momentum balance. In analogy to simple two-point

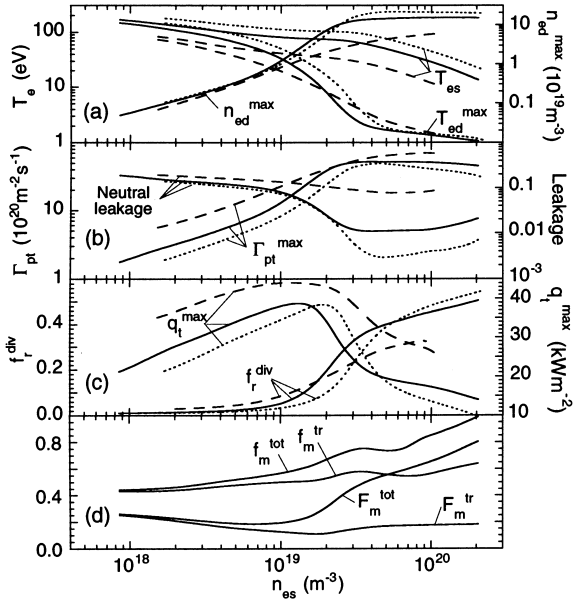

Fig. 3. Pure deuterium plasmas. Divertor plasma parameters versus the upstream density n_{es} (at point C in Fig. 2) at a power outflow from the core of $P_c = 220$ kW. Solid, dashed or dotted lines indicate medium, high or low field line pitch at the edge, respectively (see text). T_{es}, T_{ed}^{max}, n_{ed}^{max} Γ_{pt}^{max}, q_t^{max} and f_r^{div} are the upstream and downstream electron temperatures, the peak downstream density, the maximum particle flux and the peak power load onto the target, and the divertor radiated power fraction, respectively. F_m and f_m are integral (SOL + private sector) and local (along the flux tube just inside the island separatrix) momentum loss faktors, respectively. Upper indices indicate total losses (tot) and losses by momentum radial transport (tr, definitions see text).

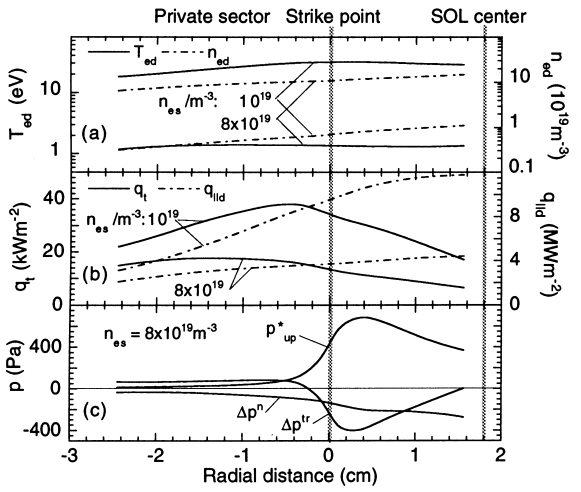

Fig. 4. Pure deuterium plasmas. (a,b) Downstream parameter radial profiles (along line HJ in Fig. 2) for an attached and a detached scenario at medium field line pitch. q_{lld} is the downstream parallel power flux, other symbols as in Fig. 3(c) Upstream total plasma pressure P_{up}^* profile (along line GEF in Fig. 2) and pressure losses due to momentum transport (Δp^{tr}) and friction with neutrals (Δp^n) at detachment.

models [14], we define integral momentum loss factors for the SOL+PS region as

$$F_{\mathrm{m}}^{\mathrm{tot}} = \int_{\mathrm{SOL+PS}} (S_{\mathrm{m}\|} + \nabla_{\perp} \cdot \Gamma_{\mathrm{m}\|})\, \mathrm{d}z\, \mathrm{d}\Psi / \int_{\mathrm{up}} p_{\mathrm{up}}^{*}\, \mathrm{d}\Psi, \qquad (1)$$

with $S_{\mathrm{m}\|}, \Gamma_{\mathrm{m}\|}, z$ and Ψ being the volume source or sink of parallel momentum due to friction with neutrals (charge exchange, ionization), the radial flux of parallel momentum (convective + conductive), the coordinate parallel to B, and the magnetic flux, respectively. $p_{\mathrm{up}}^{*} = n_{\mathrm{e,up}} T_{\mathrm{e,up}} (1+\gamma M^2)$ (with γ the adiabatic coefficient and M the Mach number) is the plasma pressure at the upstream position along line GEF in Fig. 2 (in analogy to a tokamak x-point divertor entrance). Loss factors $F_{\mathrm{m}}^{\mathrm{tr}}$ considering only momentum transport were obtained by omitting $S_{\mathrm{m}\|}$ in (1); the difference between both factors stands for the losses by friction with neutrals. Corresponding local loss factors f_{m} (along a flux tube) were obtained by substituting the integration over ψ by multiplication with the corresponding flux increment $\Delta\Psi$. As Fig. 3(d) shows, there are big differences between integral and local loss factors. At detachment, the integral losses are dominated by friction with neutrals. The divergence term in Eq. (1) contributes about 20–30% (mainly transported to the closed island range where it becomes balanced by parallel viscosity). It leads, however, to strong local losses along the flux tube range with maximum upstream pressure (just inside the island separatrix) over the whole density range as it is indicated by the respective local loss factor $f_{\mathrm{m}}^{\mathrm{tr}}$, and to pressure increase in the PS. This momentum redistribution superimposed to a nearly homogeneous concentration of momentum sinks by neutrals within the SOL range (see respective local pressure losses Δp^{tr} and Δp^{n} in Fig. 4(c)) strongly flattens the downstream pressure profiles and supports the formation of layer detachment.

Modifying the field line pitch within the divertor region changes the field line connection lengths relative to the parallel gradient lengths, and by this the role of parallel transport relative to the cross field (radial) transport. At high pitch (dashed lines in Fig. 3), T_{es} is decreased by more than a factor of 2. The intermediate high recycling scenario vanishes, the leakage for neutrals is about 10%, and detachment is less pronounced. From downstream parameter radial profiles (not shown) it is inferred, that the 2D smoothing effects mentioned are less efficient, but in the detached state the momentum sinks by neutrals are now peaked close to the strike line which finally leads to similarly flat $q_{\|\mathrm{d}}$ profiles at highest density as with median pitch. The target peak load is, however, less reduced (Fig. 3(c)), and the density limit for stationary operation is decreased. Low pitch (dotted lines in Fig. 3) has the opposite effect. The onset of detachment is shifted to slightly higher density, the leakage for neutrals is favourably reduced (about 0.3%), and the 2D features accentuated above become stronger developed but do not yet lead to qualitatively new scenarios. These results indicate that low pitch is basically preferable, but pitch variations within the accessible range may provide a 'knob' to optimize scenarios with transport coefficients (not too strongly) deviating from the above assumptions.

Deuterium plasmas with carbon as intrinsic impurity. Applying the picture of coupled momentum and impurity radiation losses [14], one expects the same qualitative behaviour also for deuterium plasmas with carbon which is indeed reproduced by the results. As Fig. 5 shows, stable detachment sets in at $n_{\mathrm{es}} \approx 2 \times 10^{19}$ m^{-3} and extends to 7×10^{19} m^{-3}. Similar to the pure deuterium case, it is partial in the sense that Γ_{pt} saturates but does not break off (Fig. 5(b)). The divertor radiated power fraction $f_{\mathrm{rC}}^{\mathrm{div}}$ due to carbon line radiation reaches up to 80%; the main part comes from the SOL region. Deuterium radiation contributes about 10% (Fig. 5(c)); energy losses due to charge exchange (not shown) are negligible. The ionization and radiation fonts are found to remain nearly parallel to the target indicating layer type detachment without strong profile changes also at these conditions. In analogy to the pure deuterium case, the development of the integral and local momentum loss factors in Fig. 5(d) as well as the downstream parameter radial profiles in Fig. 6(a) and (b) demonstrate

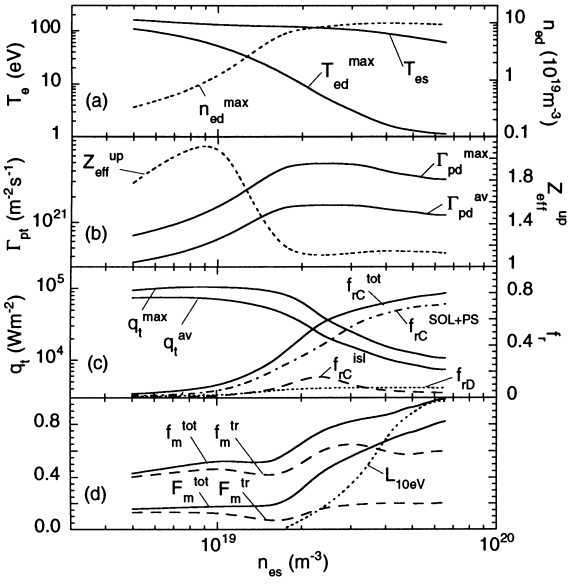

Fig. 5. Plasmas with carbon as intrinsic impurity. Divertor plasma parameters versus n_{es} at medium pitch and $P_{\mathrm{c}} = 600$ kW. Lower indices in (c) denote the total line radiation from carbon (C) or deuterium (D); the upper index 'isl' denotes the contribution from the closed island range. $L_{10\,\mathrm{eV}}$ (d) indicates the shift of the $T_{\mathrm{e}} = 10$ eV line (ionization and radiation front) from the target ($L_{10\,\mathrm{eV}} = 0$) towards the x-point position $L_{10\,\mathrm{eV}} = 1$). Other symbols as in Fig. 3.

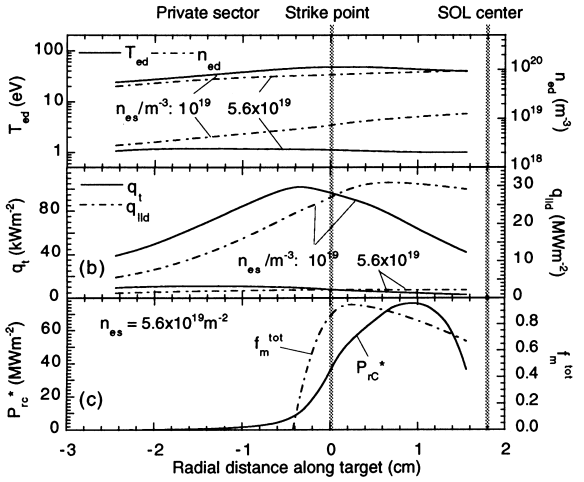

Fig. 6. Plasmas with carbon as intrinsic impurity. (a, b) Downstream parameter radial profiles for an attached and a detached scenario. Symbols as in Fig. 4. (c) Radial distribution of momentum losses f_m^{tot} (by momentum transport + friction with neutrals) and energy losses P_{rC^*} by carbon radiation (total emissivity integrated up along flux tubes).

again the strong effects of radial transport. The T_{ed} profiles are flat even before detachment, n_{ed} and $q_{\|d}$ are maximum within the SOL range between the two strike points. Momentum losses due to the superimposed effects of momentum radial transport and friction with neutrals as well as radiative losses concentrate at this latter region (Fig. 6(c), Fig. 7) thus leading to nearly homogeneous detachment over this radial range.

5. Summary and conclusions

The B2-EIRENE code package was applied to a prototypical W7-AS island divertor configuration. The divertor operational regimes are found to pass through the same sequence of states from low recycling to detachment as in a tokamak x-point divertor, thus demonstrating the proof of principle for successful operation. The power exhaust properties and the onset of detachment can be positively influenced by the choice of the field line pitch at the edge which affects the efficiency of radial relative to parallel transport. Small pitch has the benefits of good shielding of the main plasma against neutrals and of strong momentum losses close to the island separatrix due to momentum radial transport which reduces the peak power load and supports detachment. Detachment is generally layer-like which may, similar to horizontal targets in tokamak divertors, implicate a somewhat reduced SOL and therewith global density limit. Widening of the operational window

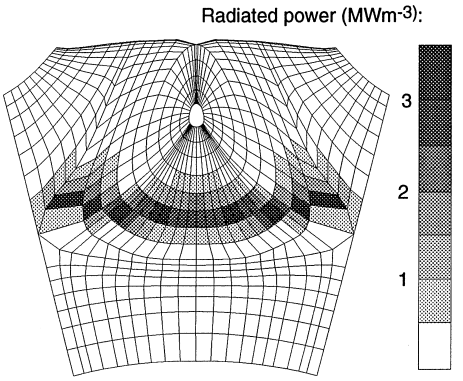

Fig. 7. 2D distribution of the carbon total line emissivity for a detachment scenario at $n_{es} = 5.6 \times 10^{19}$ m^{-3}.

should, however, be possible by optimizing the target geometry for preferential reflection of neutrals and restriction of detachment to the strike point vicinity (like e.g. in ASDEX Upgrade). Corresponding sensitivity studies are planned.

It is conjectured that basic elements of this picture are not strongly changed by 3D effects like varying flux tube cross sections and helically discontinuous target plates. This is, however, speculative at present. More information is expected from the planned divertor experiment in W7-AS supported by a 3D (Monte Carlo) edge transport code which under development [7,8].

References

[1] A. Komori et al, J. Nucl. Mater. 241–243 (1997) 967.
[2] P. Grigull et al., J. Nucl. Mater. 241–243 (1997) 935.
[3] F. Sardei et al., J. Nucl. Mater. 241–243 (1997) 135.
[4] B.J. Braams, A multifluid code for simulation of the edge plasma in tokamaks, Report No. (NET) EUR-FU/XII-80/87/68, Comm. of the EC, Brussels, 1987.
[5] D. Reiter, The EIRENE Code, Version January'92, Users Manual, Report No. 2599, Institut für Plasmaphysik, Association EURATOM-KFA, 1992.
[6] R. Schneider et al., J. Nucl. Mater. 196–198 (1992) 810.
[7] Y. Feng et al., J. Nucl. Mater. 241–243 (1997) 930.
[8] Y. Feng et al., these Proceedings.
[9] H. Renner et al., J. Nucl. Mater. 241–243 (1997) 946.
[10] G. Herre et al., J. Nucl. Mater. 241–243 (1997) 241.
[11] P. Grigull et al., in: The Tenth Int. Conf. on Stellarators, IAEA Technical Meeting, Madrid, Spain, 1995, Report EUR-CIEMAT, vol. 30, 1995, p. 73.
[12] K.-U. Riemann, J. Phys. D 24 (1991) 493.
[13] W. Eckstein, Report IPP 9/117, Garching, March, 1998.
[14] K. Borrass, D. Coster, R. Schneider, Controlled Fusion and Plasma Physics (Proc. 25th Eur. Conf., Berchtesgaden, 1997), vol. 21A, Part IV (1997) p. 1461.